Electrokinetic particle separation in a single-spiral microchannel

2014 J. Micromech. Microeng. 24 115018

(http://iopscience.iop.org/0960-1317/24/11/115018)

IOP Publishing Journal of Micromechanics and Microengineering
J. Micromech. Microeng. **24** (2014) 115018 (7pp) doi:10.1088/0960-1317/24/11/115018

Electrokinetic particle separation in a single-spiral microchannel

John DuBose, Junjie Zhu, Saurin Patel, Xinyu Lu, Nathaniel Tupper, John M Stonaker and Xiangchun Xuan

Department of Mechanical Engineering, Clemson University, Clemson, SC 29634-0921, USA

E-mail: xcxuan@clemson.edu

Received 21 June 2014, revised 4 September 2014
Accepted for publication 15 September 2014
Published 24 October 2014

Abstract

The efficient separation of discrete particle species is a topic of interest in numerous research fields for its practical application to problems encountered in both academia and industry. We have recently developed an electrokinetic technique that exploits the curvature-induced dielectrophoresis (C-iDEP) to continuously sort particles by inherent properties in asymmetric double-spiral microchannels. Herein we demonstrate that a single-spiral microchannel is also sufficient for a continuous-flow sheathless electrokinetic particle separation. This method relies on C-iDEP to focus particles to a tight stream and the wall-induced electric lift to manipulate the aligned particles to size-dependent equilibrium positions, both of which happen simultaneously inside the spiral. A theoretical model is developed to understand this size-based separation, which has been implemented for both a binary mixture and a ternary mixture of colloidal particles. The obtained analytical formulae predict with a close agreement both the experimentally measured particle center–wall distance and the necessary electric field for a complete particle focusing in the spiral.

Keywords: microfluidics, electrokinetics, dielectrophoresis, single spiral, separation

S Online supplementary data available from stacks.iop.org/JMM/24/115018

(Some figures may appear in colour only in the online journal)

1. Introduction

The efficient separation of discrete particle species is a topic of interest in numerous research fields for its practical application to problems encountered in medicine, agriculture, food technology, and pharmaceuticals etc. To achieve this goal, microfluidic devices present a viable alternative to larger analytical devices through advantages in efficiency, resolution, portability and cost [1–3]. Batch-wise separation techniques such as filtration [4], chromatography [5], electrophoresis [6], and field-flow fractionation [7] have historically been favored. However, in recent years, the concept of continuous-flow separation has become increasingly explored and developed [8–10]. This technique involves the continuous injection of a stream of particles into a microchannel so that an angular force may act upon the particles locally or throughout the channel. Such forces can be externally applied which cover electrical [11, 12], optical [13], magnetic [14], acoustic [15], and hydrodynamic [16] fields. They can also be induced internally, among which deterministic lateral displacement [17], hydrodynamic filtration [18], hydrophoresis [19], and inertial microfluidics [20] have each been demonstrated to separate particles and cells.

The most widely utilized among the forces for particle separation is dielectrophoresis (DEP), which arises from the interaction of an induced or intrinsic electric dipole in the particle and a non-uniform electric field [21]. Traditionally electric field gradients have been actively created by imbedded electrodes, either planar [22, 23] or three-dimensional [24, 25], within the microchannel itself. Particles or cells are reoriented according to the magnitude and frequency of the imposed ac electric field, making this technique generally effective for a range of particle species [26, 27]. Dynamic ac-DEP channels of this nature have distinct disadvantages including the fabrication complexity and surface degradation of in-channel microelectrodes [28]. To overcome some of these difficulties,

external electrode structures have been proposed which do not make contact with the channel, but that preserve the influence of ac fields through the use of dielectric barriers [29]. An alternative to the electrode-based DEP (eDEP) technique makes use of insulating channel geometries to form non-uniform electric fields. Because they are made of the same material as the channel substrate, insulating structures such as hurdles [30–34] and posts [35–37] can squeeze electric field lines to create local electric field gradients [38]. Such an insulator-based DEP (iDEP) technique avoids the issues caused by the in-channel electrodes. More importantly, it can use dc electric fields to pump the suspending fluid and manipulate the suspended particles simultaneously [39, 40].

Recently our group has developed a new type of iDEP technique that relies on the inherent electric field gradients induced within microchannel turns [41–45]. This technique, which we termed curvature-induced DEP (C-iDEP), has been demonstrated to continuously separate particles based on the difference of size [46], charge, or both [47] in double-spiral microchannels. It exploits C-iDEP to focus a particle mixture to a tight stream in the first spiral without sheath flows and subsequently displace particles to property-dependent flow paths in the second spiral. Very recently this technique has also been utilized by out group to separate peanut-shaped particles from spherical particles of similar volumes in an asymmetric double-spiral microchannel [48]. We demonstrate in this work that a single-spiral microchannel is also sufficient for a continuous-flow sheath-free electrokinetic separation of particles by size. A theoretical model is developed to understand and predict this separation, which turns out to be the result of the competition between the C-iDEP focusing and the wall-induced electric lift in the spiral.

2. Experiment

2.1. Microchannel fabrication

The single-spiral microchannel was fabricated via a standard soft lithography technique. Several molds of the microchannel were manufactured initially for repeated use after each experimental trial. To create the channel photomasks for the specified geometry, drawings made using AutoCAD® software were printed on a transparent plastic film (CAD/Art Services, Bandon, OR). After glass slides were thoroughly cleaned, photoresist (SU-8 25, MicroChem Corp, Newton, MA) was uniformly dispersed to a specific depth of 25 μm using a programmed spin-coater (WS-400E-NPP-Lite, Laurell Technologies, North Wales, PA) which ramped to a final speed of 2000 rpm for 25 s. Once the coating was complete, each slide was baked in a two-step process from 65 °C for 3 min to 95 °C for 7 min on two hotplates (HP30A, Torrey Pines Scientific, San Marcos, CA). Then, with the photomask applied to the top of the photoresist coating, the slide was exposed to a UV treatment (ABM Inc., San Jose, CA) to create the channel imprint. The intensity and exposure time used were specific to the designated photoresist thickness. Directly following the UV treatment, the photoresist film was again baked for 1 min at 65 °C and finally for 3 min at 95 °C. The slides were then developed in an SU-8 developing solution for 5 min and rinsed with isopropyl alcohol to reveal the finished microchannel mold.

Once dry, the channel molds were placed in individual Petri dishes and covered with liquid polydimethylsiloxane (PDMS). Bubbles created in the PDMS during its mixing and pouring were subsequently removed using a vacuum oven for 15 min (13-262-280A, Fisher Scientific, Fair Lawn, NJ). The PDMS was then cured for two hours at 70 °C in a gravity convection oven (13-246-506GA, Fisher Scientific, Fair Lawn, NJ). Once removed from the oven, the Petri dishes were allowed to cool. Then, using a scalpel, the channels were cut from and peeled off of the molds. At each of the channel outlets, holes were punched using a syringe with a needle of diameter of 1.65 mm to serve as reservoirs. After taking care to ensure that no debris remained on the surface, the channel side and a cleaned glass slide were plasma treated (PDC-32 G, Harrick Scientific, Ossining, NY) for 1 min and 30 s. Once removed, the clean slide and the channel were immediately bonded and heated on a hot plate for 45 s at 120 °C to ensure a strong, permanent bond. When the channel had cooled sufficiently, deionized water was introduced through the reservoirs via capillary action to preserve the hydrophilic properties of the channel walls.

A top-view picture of the fabricated single-spiral microchannel is illustrated in figure 1(*a*), which consists of three 50 μm wide loops with the inlet reservoir at the center of the loops. The diameter of the most inner loop is 4 mm and the loop-to-loop distance is maintained at 200 μm. The length of the spiral from the inlet reservoir to the point of divergence at the outlet is 4 cm. The three outlet branches are each 5 mm long and 100 μm wide. The entire channel has a uniform depth of 25 μm. Four equal-sized pipette tips were inserted into the inlet and outlet reservoirs (all of 2 mm in diameter) each for an easy electrical connection.

2.2. Particle manipulation

Spherical polystyrene particles (Sigma-Aldrich, USA) of 5 μm, 10 μm, and 15 μm in diameter, respectively, were used in our experiment. Depending upon the required application, one (for particle focusing), two (for binary particle separation), or three (for ternary particle separation) sizes of particles were re-suspended in 1 mM phosphate buffer at a concentration of 10^6–10^7 particles ml^{-1} for each. This solution has a relatively low electric conductivity of 210 μS cm^{-1} and has been regularly used in our previous studies on electrokinetic particle manipulations [46–49]. These works demonstrate that Joule heating effects are insignificant as long as the applied electric field is kept no more than 500 V cm^{-1} [46–50]. A small amount of Tween 20 (0.5% v/v, Fisher Scientific) was added to the particle suspensions. It was found to slightly slow down the electrokinetic particle motion, but help reducing significantly the particle-particle and particle–wall adhesions. A dc power source (Glassman High Voltage), along with a custom circuit for discrete outlet voltage control, was used to supply electric field to the microchannel. Pressure-driven fluid and particle motions were minimized by carefully balancing the liquid

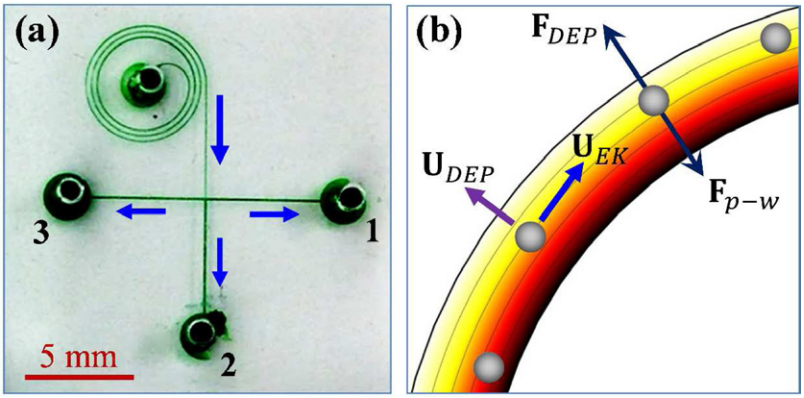

Figure 1. (*a*) Top-view image of the single-spiral microchannel (filled with green food dye for visualization) used in particle focusing and separation experiments. The three outlets are numbered for references in the text and the block arrows indicate the flow directions; (*b*) Illustration of the mechanism of electrokinetic particle separation in a curving microchannel due to the C-iDEP focusing and the particle size-dependent equilibrium position of the focused particles. The legends on panel (*b*) are: $\boldsymbol{U}_{\mathrm{DEP}}$, dielectrophoretic particle velocity; $\boldsymbol{U}_{\mathrm{EK}}$, electrokinetic particle velocity; $\boldsymbol{F}_{\mathrm{DEP}}$, curvature-induced dielectrophoretic force; $\boldsymbol{F}_{\mathrm{p-w}}$, wall-induced electric lift force (more details are given in section 3.1). The background shows the electric field lines and contour (the darker the color, the higher the magnitude).

levels in the reservoirs prior to each test and by continuously running the experiment for no more than 5 min each. Videos and images were taken with an inverted microscope camera system (Nikon Eclipse TE2000U, Nikon Instruments) and post-processed using the Nikon imaging software. The electrokinetic particle mobility, i.e., electrokinetic velocity per unit electric field [cf., equation (3)], was measured by tracking single particles in the straight part of the microchannel. A given low electric field was used in this measurement to avoid both Joule heating and DEP effects [51]. The three types of particles used in our experiment were found to have a similar electrokinetic mobility value of $2.5 \times 10^{-8}\,\mathrm{m^2 V^{-1} s^{-1}}$.

3. Theory

3.1. Mechanism of electrokinetic focusing and separation in a single-spiral

As indicated by the contour (see the background color, the darker the larger magnitude) in figure 1(*b*), the electric field in a spiral microchannel attains the maximum and minimum values near the inner and outer walls, respectively. These electric field gradients induce a dielectrophoretic force, $\boldsymbol{F}_{\mathrm{DEP}}$, on the suspended particles [52, 53]

$$\mathbf{F}_{\mathrm{DEP}} = -2\pi\varepsilon_{\mathrm{f}} a^3 (\mathbf{E}\cdot\nabla\mathbf{E}) = -2\pi\varepsilon_{\mathrm{f}} a^3 \frac{E^2}{\mathfrak{R}}\mathbf{n}, \tag{1}$$

where ε_{f} is the permittivity of the suspending fluid, a is the radius of spherical particles, $\boldsymbol{E}$ is the electric field vector with a magnitude of E, $\mathfrak{R}$ is the radius of curvature of electric field lines (similar to fluid streamlines [54]) in figure 1(*b*), and $\boldsymbol{n}$ is the unit normal vector pointing towards the center of curvature. Note that in equation (1) we have assumed −0.5 for the so-called Clausius–Mossotti factor [21]. It is because the electrical conductivities of polystyrene particles used in our experiment (which are $8.0\,\mu\mathrm{S\,cm^{-1}}$, $4.0\,\mu\mathrm{S\,cm^{-1}}$, and $2.6\,\mu\mathrm{S\,cm^{-1}}$ for 5 μm, 10 μm, and 15 μm-diameter particles, respectively, calculated via the equation suggested by Ermolina and Morgan [55]) are each much lower than that of the suspending fluid (which is $210\,\mu\mathrm{S\,cm^{-1}}$, measured directly). Therefore, these particles experience negative DEP, as indicated by the negative sign in equation (1), and are pushed away from the inner wall of the spiral at a velocity, $\boldsymbol{U}_{DEP}$ [see figure 1(*b*)] [52, 53],

$$\mathbf{U}_{\mathrm{DEP}} = -\frac{a^2\varepsilon_{\mathrm{f}}}{3\eta_{\mathrm{f}}}\frac{E^2}{\mathfrak{R}}\mathbf{n}, \tag{2}$$

where η_{f} is the fluid viscosity. This cross-stream dielectrophoretic motion competes with the stream-wise electrokinetic transport of particles, $\boldsymbol{U}_{\mathrm{EK}}$ [56],

$$\mathbf{U}_{\mathrm{EK}} = \frac{\varepsilon_{\mathrm{f}}\left(\zeta_{\mathrm{p}} - \zeta_{\mathrm{w}}\right)\mathbf{E}}{\eta_{\mathrm{f}}} = \mu_{\mathrm{EK}} E\mathbf{s} \tag{3}$$

where ζ_{p} is the zeta potential of particles, ζ_{w} is the zeta potential of the microchannel wall, $\mu_{\mathrm{EK}} = \varepsilon_{\mathrm{f}}(\zeta_{\mathrm{p}} - \zeta_{\mathrm{f}})/\eta_f$ is the electrokinetic particle mobility, and $\boldsymbol{s}$ is the unit vector tangential to the electric field line. The resulting transverse particle deflection is expressed as [47]

$$\mathrm{Deflection} = U_{\mathrm{DEP}}\frac{\mathfrak{R}\theta}{U_{\mathrm{EK}}} = \frac{a^2}{3\left(\zeta_{\mathrm{p}} - \zeta_{\mathrm{w}}\right)} E\theta, \tag{4}$$

where θ is the opening angle of the spiral. The consequence of this C-iDEP 'Deflection' is a focused particle stream flowing near the outer wall of the spiral microchannel if the applied electric field is sufficiently large or the spiral is sufficiently long (e.g., of multiple loops).

However, the focused particles are unable to align against the outer wall due to a wall-induced electric force. This DEP-resembled lift force, $\boldsymbol{F}_{\mathrm{p-w}}$, results from the asymmetric electric field around an insulating particle when the particle is moving close to a dielectric wall [57–60],

$$\mathbf{F}_{\mathrm{p-w}} = \frac{3\pi}{16}\left(\frac{a}{h}\right)^4 \varepsilon_{\mathrm{f}} a^2 E^2 \mathbf{n}, \tag{5}$$

where h is the perpendicular distance between the particle center and the wall, and $\boldsymbol{n}$ is the unit normal vector of the outer wall that points towards the fluid and is consistent

with the definition in equation (2). It is important to note that equation (5) was obtained for a particle near a plane wall [57], which, however, is still valid for the current case because the particle radius ($a \leq 7.5\,\mu$m) is much smaller than the radius of curvature of the spiral ($\mathfrak{R} = 2.5$ mm). Such an electric field-originated lift force is significantly larger than the hydrodynamic-originated initial lift force [61] because the channel Reynolds number is less than 1 and the particle Reynolds number is far less than 1 in typical electrokinetic flows [56]. It is also far greater than the centrifugal force experienced by the particle in the spiral due to the very small particle Reynolds number and the closely matched fluid and particle densities [62]. Therefore, the equilibrium position, h_{eq}, of the electrokinetically focused particles is determined by the balancing of the dielectrophoretic force, $\boldsymbol{F}_{DEP}$, in equation (1) and the particle–wall interaction force, $\boldsymbol{F}_{p-w}$, in equation (5), which yields

$$h_{eq} = \left(\frac{3}{32} a^3 \mathfrak{R}\right)^{1/4}. \tag{6}$$

This equilibrium particle center–wall distance, h_{eq}, increases for larger particles, and is found independent of the applied electric field in theory. It is, however, very important to note that equation (6) is only applicable to particles that have been fully deflected by C-iDEP in the spiral, i.e., those that can be focused to a single file near the outer wall of the spiral (see figure 1(*b*)). For this to happen, the particle *Deflection* in equation (4) should fulfill the following condition,

$$\text{Deflection} = \frac{a^2\theta}{3\left(\zeta_p - \zeta_w\right)} E \geq w - a - h_{eq}, \tag{7}$$

where w is the width of the spiral channel and the particle size, a, is included to consider the steric effects. Thus, the minimum electric field for a full electrokinetic particle focusing in the single-spiral microchannel can be estimated from equation (7) as,

$$E_{min} = \frac{3\left(\zeta_p - \zeta_w\right)\left(w - a - h_{eq}\right)}{a^2\theta}, \tag{8}$$

which is apparently a strong function of particle size. The smaller particles, the higher electric field is required for a complete focusing by C-iDEP.

3.2. Theoretical predictions under the experimental conditions

Considering that the radius of curvature for the most outer loop in our single-spiral microchannel (see figure 1(*a*)) is $\mathfrak{R}$ = 2.5 mm, the estimated values of h_{eq} are 7.8 μm, 13.1 μm, 17.7 μm for 5 μm, 10 μm, and 15 μm-diameter particles, respectively. This dependence of h_{eq} on particle size enables the continuous electrokinetic separation of particles in a single-spiral microchannel to be demonstrated in the next section. Also, with the experimentally measured electrokinetic mobility, i.e., $\mu_{EK} = 2.5 \times 10^{-8}\,m^2\,(V^{-1}\,s^{-1})$ in equation (3), we calculated the zeta potential difference, $(\zeta_p - \zeta_f)$, as 35.3 mV for all three sizes of particles. Hence, the minimum electric fields, E_{min}, for a complete electrokinetic particle focusing in the fabricated three-loop ($\theta = 6\pi$) spiral (see figure 1(*a*)) can be estimated from equation (8), which was found to be 357.1 V cm^{-1}, 71.7 V cm^{-1} and 24.8 V cm^{-1} for 5 μm, 10 μm, and 15 μm particles, respectively. This theoretical analysis indicates that a minimum electric field of around 350 V cm^{-1} must be used in our experiment in order to achieve the electrokinetic separation of these particles via the particle-size dependent equilibrium position, h_{eq}. It also poses a size limit on the smallest particles that can still be effectively separated using the proposed single-spiral microchannel. Being a second-order function of particle size, the minimum electric field in equation (8) can easily go beyond 1000 V cm^{-1} for particles with a diameter of less than 2 μm. Such a high electric field can easily draw significant Joule heating to the fluid and cause damages to both the sample and the device [63–65].

4. Results and discussion

4.1. Particle-size dependent equilibrium position

Figure 2 demonstrates the C-iDEP focusing of pure 5 μm (*a*1, *a*2) and pure 10 μm (*b*1, *b*2) particles, respectively, in 1 mM phosphate buffer through the single-spiral microchannel. The imposed dc voltage at the channel inlet was 1600 V and all outlets were grounded in both cases, leading to an average electric field of 350 V cm^{-1} in the spiral. This voltage or field was found to be the minimum in order to completely focus both types of particles in the spiral, which agrees closely with the above theoretical analysis. At the inlet of the channel (data not shown), particles are evenly distributed throughout the solution. As they travel through the spiral, particles undergo a negative DEP force which progressively focuses them to the region of lowest electric field intensity on the outer wall of the channel. The degree to which particles are focused depends on the Deflection in equation (4), which increases for larger particles. This trend can be viewed from the particle images taken at the spiral section of the channel in figures 2(*a*1) and (*b*1). The same figure also demonstrates that the focused particles are unable to reach the outer channel wall due to the wall-induced electrical repulsion force.

After the final loop of the spiral, 10 μm particles are apparently a little farther away from the outer channel wall than 5 μm particles as evidenced from the zoom-in snapshot images in the inset of figures 2(*a*1) and (*b*1). The equilibrium particle center–wall distances, i.e., h_{eq}, were measured to be approximately 9 μm and 15 μm for 5 μm and 10 μm particles, respectively, both of which appear to be consistent with the estimated values via equation (6) in the Theory section. We have also measured the particle center–wall distances, h_{eq}, for 10 μm particles at the applied dc voltages of 1200 V and 2000 V, both of which produce an electric field larger than the minimum value predicted in equation (8) for a complete electrokinetic focusing of 10 μm particles in the spiral. A roughly identical h_{eq} to that under 1600 V (see figure 2(*b*1)) was obtained in both cases, which validates the theoretical prediction of equation (6) that the equilibrium position of fully focused particles in the spiral is dependent of the applied electric field.

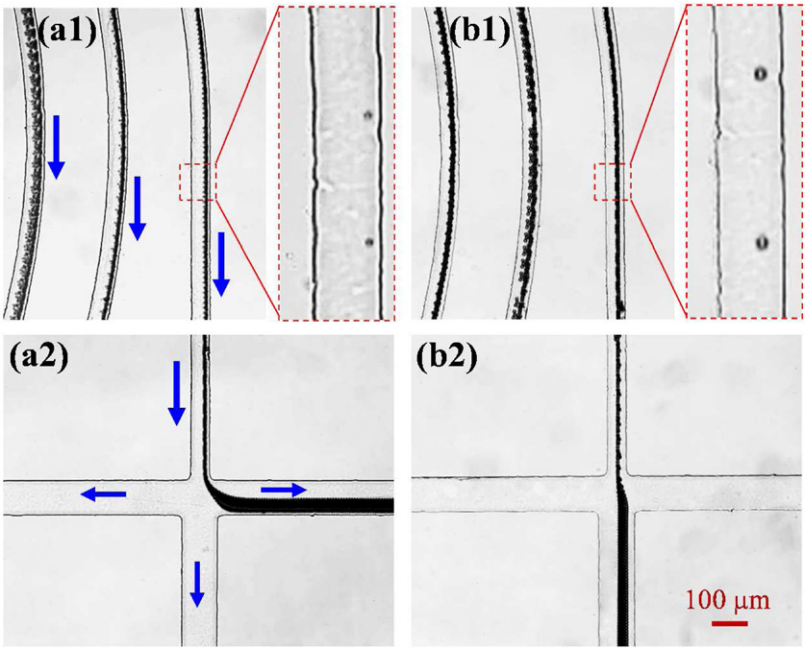

Figure 2. Illustration of C-iDEP focusing of pure 5 μm ($a1$, $a2$) and pure 10 μm ($b1$, $b2$) particles, respectively, in the single spiral microchannel and the size-dependent separation distance between the focused particles and the channel wall. ($a1$, $b1$) show the superimposed images of the two particle species taken at the spiral section of the channel with the insets being the zoom-in snapshot images. ($a2$, $b2$) show the superimposed images of the two particles taken at the trifurcation of the channel. In each case, the imposed voltage at the inlet was 1600 V dc and all outlets were grounded. The block arrows indicate the particle/fluid moving directions in the channel.

The particle–wall separation distance continually increases in the straight section immediately following the spiral part of channel. It is because C-iDEP vanishes ($\mathfrak{R} \rightarrow \infty$ in equations (1) and (2)) while the particle–wall interaction force, $\boldsymbol{F}_{\text{p–w}}$, remains to push particles towards the channel centerline [58, 59]. Right before the point of divergence at the channel outlet, the particle center–wall distances for 5 μm and 10 μm particles were measured to be approximately 14 μm and 22 μm, respectively, in the 50 μm-wide channel. As the three collecting branches are identical and all grounded, the fluid flow is evenly divided at the channel trifurcation. Therefore, the focused 5 μm and 10 μm particles are found to travel into the first (right-most) and second (center) outlets (see the numbering in figure 1(a)) as illustrated in figure 2($a2$) and figure 2($b2$), respectively.

4.2. Binary particle separation

The observed discrete trajectories for particles of dissimilar sizes in figure 2 indicate the potential to electrokinetically separate them based up size in a single-spiral microchannel. As seen from the superimposed image in figure 3, a binary mixture of 5 μm and 10 μm particles are continuously sorted under the same working conditions as those for the C-iDEP focusing in figure 2. Note that the multi-trajectories of the smaller particles on the image in figure 3 are mainly because the presence of one or more neighboring particles disturbs the position of each particle, especially significant when they travel into the trifurcation at a slowed speed. The two particle species can be effectively separated at a purity of nearly 100% for both the first (right-most)

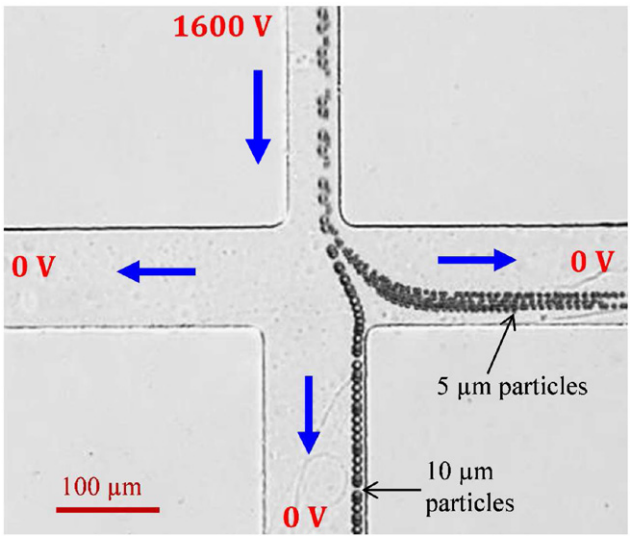

Figure 3. Superimposed image showing the electrokinetic separation of a binary mixture of 5 μm and 10 μm particles in the single-spiral microchannel. The dc voltages imposed to the inlet and outlet reservoirs are as labeled on the image. The block arrows indicate the particle/fluid moving directions in the channel. A video of this separation is available in the supplementary data stacks.iop.org/JMM/24/115018

and second (center) outlet reservoirs. This separation can also be implemented using a smaller dc electric field across the channel, for which, however, bias voltages must be used at the outlet reservoirs to tune the flow splitting at the trifurcation. For example, a 1400 V dc voltage at the channel inlet with all three outlets grounded is only able to fully focus and deflect 10 μm particles

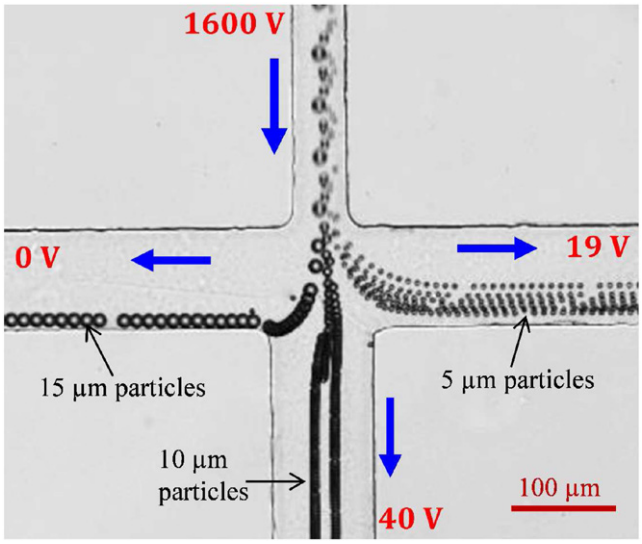

Figure 4. Superimposed image showing the electrokinetic separation of a ternary mixture of 5 μm, 10 μm, and 15 μm particles in the single-spiral microchannel. The dc voltages imposed to the inlet and outlet reservoirs are as labeled on the image. The block arrows indicate the particle/fluid moving directions in the channel. A video of this separation is available in the supplementary data stacks.iop.org/JMM/24/115018

to the equilibrium position, yielding an incomplete separation of 5 μm particles in the second (center) outlet (data not shown). However, a 9 V dc bias voltage at the third (left-most) outlet is able to alter the particle trajectories and force 5 μm and 10 μm particles to migrate into the first (left-most) and second (center) outlets, respectively (data not shown). The measured average speed of each type of particles in the spiral part is about 1 mm s^{-1} for the separation shown in figure 3. The estimated volume flow rate of the particle suspension is around 10 μl h^{-1}, which is relatively low as compared to other microfluidics-based particle separation methods. However, the ease of control greatly facilitates the integration of this electrical field-driven particle sorter with other functional components into lab-on-a-chip devices for handling minute samples.

4.3. Ternary particle separation

Figure 4 demonstrates the electrokinetic separation of a ternary mixture of 5 μm, 10 μm, and 15 μm particles in 1 mM phosphate buffer through the single-spiral microchannel. The dc voltage imposed to the channel inlet is still 1600 V, which is able to fully focus 15 μm particles to the equilibrium position with a particle cell-water distance of 19 μm after the final loop of the spiral. If all outlets were grounded, 15 μm particles would be pushed to the center of the straight channel before the trifurcation and inclined to travel into the second (center) outlet along with 10 μm particles. With biased electrical potentials of 19 V and 40 V, respectively, imposed at the first (right-most) and second (center) outlets, an effective sorting of the three particle species into the three outlets can be achieved as viewed from the superimposed image in figure 4. We tested the purity of this ternary particle separation by manually counting the particles in independent videos, from which the percentage of each size of particles collected into each of the three outlets was

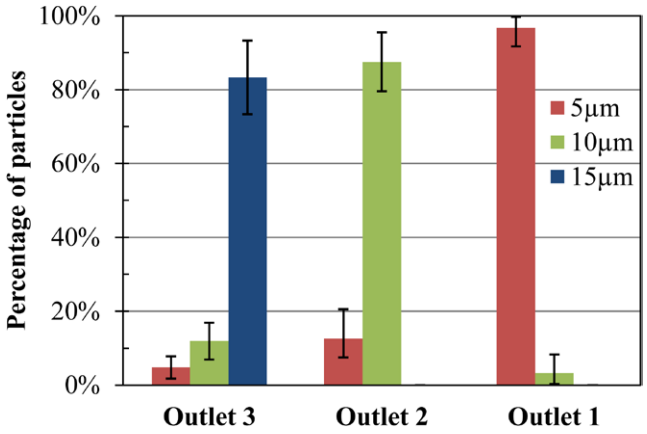

Figure 5. Column graph showing the purity test for the electrokinetic separation of a ternary mixture of 5 μm, 10 μm, and 15 μm particles in the single-spiral microchannel (see also figure 4).

calculated. More than 200 particles were counted with at least 40 particles for each species. As seen from the column plot in figure 5, 97% of the particles in outlet 1 (right-most) are 5 μm, 87% of the particles in outlet 2 (center) are 10 μm, and 83% of the particles in outlet 3 (left-most) are 15 μm. The reduced particle purities in the second and third outlets are mainly due to particle agglomerations, especially the attachment of 5 μm particles onto larger particles.

5. Conclusions

We have developed in this work a continuous-flow electrokinetic technique for particle separation in single-spiral microchannels. This sheath-free sorting method arises essentially from the particle size-dependent separation distance between the C-iDEP focused particles and the channel wall. It has been experimentally demonstrated through both a binary separation of 5 μm/10 μm particles and a ternary separation of 5 μm/10 μm/15 μm particles in the same single-spiral microchannel. We have also developed a theoretical model that considers the effects of the wall-induced dielectrophoretic force and lift force (also of electric origin). The predictions of the equilibrium particle center–wall distance, h_{eq}, from the obtained closed-form expression in equation (6) appear to agree closely with the experimental observations for particles of different sizes and as well the same size of particles under different electric fields. Moreover, the theoretically predicted minimum electric field in equation (8) is also consistent with the value used in the experiment in order for a complete electrokinetic focusing of particles in the single-spiral. However, the strong size-dependence of this minimum electric field dictates that the proposed device is best suited for sorting a few to tens micron-sized particles. Future work can be done for particle separation based on other intrinsic properties such as surface charge or shape.

Acknowledgments

This work was supported in part by NSF under grant CBET-0853873 and by Clemson University through the SGER grant and the Creative Inquiry Program.

References

[1] Pamme N 2007 *Lab Chip* **7** 1644–59
[2] Gossett D R, Weaver W M, Mach A J, Hur S C, Tse H T, Lee W, Amini H and Di Carlo D 2010 *Anal. Bioanal. Chem.* **397** 3249–67
[3] Watarai H 2013 *Annu. Rev. Anal. Chem.* **6** 353–78
[4] Sethu P, Sin A and Toner M 2006 *Lab Chip* **6** 83–9
[5] Dainiak M B, Plieva F M, Galaev I Y, Hatti-Kaul R and Mattiasson B 2005 *Biotechnol. Prog.* **21** 644–9
[6] Kremser L, Blaas D and Kenndler E 2004 *Electrophoresis* **25** 2282–91
[7] Giddings J C 1993 *Science* **260** 1456–65
[8] Kulrattanarak T, van der Sman R G M, Schroen C G P and Boom R M 2008 *Adv. Colloid. Interface Sci.* **142** 53–65
[9] Lenshof A and Laurell T 2010 *Chem. Soc. Rev.* **39** 1203–17
[10] Autebert J, Coudert B, Bidard F, Pierga J, Descroix S, Malaquin L and Viovy J 2012 *Methods* **57** 297–307
[11] Zhang C and Manz A 2003 *Anal. Chem.* **75** 5759–66
[12] Kang Y and Li D 2009 *Microfluid. Nanofluid.* **6** 431–60
[13] Kim S B, Yoon S Y, Sung H J and Kim S S 2008 *Anal. Chem.* **80** 2628–30
[14] Zhu T, Cheng R, Lee S A, Rajaraman E, Eiteman M A, Querec T D, Unger E R and Mao L 2012 *Microfluid. Nanofluid.* **13** 645–54
[15] Ding X 2013 *Lab Chip* **13** 3626–49
[16] Takagi J, Yamada M, Yasuda M and Seki M 2005 *Lab Chip* **5** 778–84
[17] Huang L, Cox E C, Austin R H and Sturm J C 2004 *Science* **304** 987–90
[18] Yamada M and Seki M 2005 *Lab Chip* **5** 1233–9
[19] Choi S, Song S, Choi C and Park J K 2009 *Anal. Chem.* **81** 1964–8
[20] Di Carlo D 2009 *Lab Chip* **9** 3038–46
[21] Morgan H and Green N G 2002 *AC Electrokinetics: Colloids and Nanoparticles* (Philadelphia: Research Studies)
[22] Gascoyne P R C and Vykoukal J 2002 *Electrophoresis* **23** 1973–83
[23] Hughes M P 2002 *Electrophoresis* **23** 2569–82
[24] Martinez-Duarte R, Renaud P and Madou M 2011 *Electrophoresis* **32** 2385–92
[25] Perez-Gonzalez V H, Ho V, Kulinsky L, Madou M and Martinez-Chapa SO 2013 *Lab Chip* **13** 4642–52
[26] Pethig R 2010 *Biomicrofluidics* **4** 022811
[27] Gagnon Z R 2011 *Electrophoresis* **32** 2466–87
[28] Voldman J 2006 *Annu. Rev. Biomed. Eng.* **8** 425–54
[29] Shafiee H, Caldwell J L, Sano M B and Davalos R V 2009 *Biomed. Microdevices* **11** 997–1006
[30] Hawkins B G, Smith A E, Syed Y A and Kirby B J 2007 *Anal. Chem.* **79** 7291–300
[31] Pysher M D and Hayes M A 2007 *Anal. Chem.* **79** 4552–7
[32] Kang K, Kang Y, Xuan X and Li D 2006 *Electrophoresis* **27** 694–702
[33] Kang Y, Li D, Kalams S A and Eid J E 2008 *Biomed. Microdevices* **10** 243–9
[34] Lewpiriyawong N, Yang C and Lam Y C 2008 *Biomicrofluidics* **2** 034105
[35] Lapizco-Encinas B H, Simmons B A, Cummings E B and Fintschenko Y 2004 *Electrophoresis* **25** 1695–704
[36] Gallo-Villanueva R C, Jesús-Pérez N M, Martínez-López J I, Pacheco A and Lapizco-Encinas B H 2011 *Microfluid. Nanofluid.* **10** 1305–15
[37] Gallo-Villanueva R C, Pérez-González V H, Davalos R V and Lapizco-Encinas B H 2011 *Electrophoresis* **32** 2456–65
[38] Li M, Li WH, Zhang J, Alici G and Wen W 2014 *J. Phys. D: Appl. Phys.* **47** 063001
[39] Srivastava S K, Gencoglu A and Minerick A R 2011 *Anal. Bioanal. Chem.* **399** 301–21
[40] Regtmeier J, Eichhorn R, Viefhues M, Bogunovic L and Anselmetti D 2011 *Electrophoresis* **32** 2253–73
[41] Zhu J, Tzeng TJ, Hu G and Xuan X 2009 *Microfluid. Nanofluid.* **7** 751–6
[42] Church C, Zhu J, Nieto J, Keten G, Ibarra E and Xuan X 2010 *J. Micromech. Microeng.* **20** 065011
[43] Zhu J, Canter R C, Keten G, Vedantam P, Tzeng T J and Xuan X 2011 *Microfluid. Nanofluid.* **11** 743–52
[44] Li M, Li S B, Cao W B, Li W H, Wen W J and Alici G 2012 *J. Micromech. Microeng.* **22** 095001
[45] Li M, Li S B, Cao W B, Li W H, Wen W J and Alici G 2013 *Electrophoresis* **34** 952–60
[46] Zhu J, Tzeng T J and Xuan X 2010 *Electrophoresis* **31** 1382–8
[47] Zhu J and Xuan X 2011 *Biomicrofluidics* **5** 024111
[48] DuBose J, Lu X, Patel S, Qian S, Joo S and Xuan X 2014 *Biomicrofluidics* **8** 014101
[49] Kale A, Lu X, Patel S and Xuan X 2014 *J. Micromech. Microeng.* **24** 075007
[50] Zhu J, Sridharan S, Hu G and Xuan X 2012 *J. Micromech. Microeng.* **22** 075011
[51] Xuan X 2008 *Electrophoresis* **29** 33–43
[52] Zhu J and Xuan X 2009 *Electrophoresis* **30** 2668–75
[53] Zhu J and Xuan X 2009 *J. Colloid. Interface Sci.* **340** 285–90
[54] Santiago J G 2001 *Anal. Chem.* **73** 2353–65
[55] Ermolina I and Morgan H 2005 *J. Colloid Interface Sci.* **285** 419–28
[56] Li D 2004 *Electrokinetics in Microfluidics* (New York: Academic)
[57] Yariv E 2006 *Phys. Fluids* **18** 031702
[58] Liang L, Ai Y, Zhu J, Qian S and Xuan X 2010 *J. Colloid Interface Sci.* **347** 142–6
[59] Liang L, Qian S and Xuan X 2010 *J. Colloid Interface Sci.* **350** 377–9
[60] Kazoe Y and Yoda M 2011 *Langmuir* **27** 11481–8
[61] Di Carlo D 2009 *Lab Chip* **9** 3038–46
[62] Zhang J, Li M, Li W and Alici G 2013 *J. Micromech. Microeng.* **23** 085023
[63] Hawkins BG and Kirby BJ 2010 *Electrophoresis* **31** 3622–33
[64] Kale A, Patel S, Hu G and Xuan X 2013 *Electrophoresis* **34** 674–83
[65] Gallo-Villanueva R C, Sano M B, Lapizco-Encinas B H and Davalos R V 2014 *Electrophoresis* **35** 352–61